Lifetime measurement of the $5s5p\,^1P_1$ state in strontium

Ivana Puljić, Ana Cipriš,* Damir Aumiler, Ticijana Ban, and Neven Šantić†
Centre for Advanced Laser Techniques, Institute of Physics, Bijenička Cesta 46, 10000 Zagreb, Croatia

(Received 13 January 2025; accepted 20 February 2025; published 11 March 2025)

We present a direct lifetime measurement of the $5s5p\,^1P_1$ state of strontium using time-correlated single-photon counting of laser-induced fluorescence in a hot atomic beam. To achieve fast switch-off times and a high signal-to-noise ratio, we excite the strontium atoms with a femtosecond pulsed laser at approximately 461 nm and collect the fluorescence onto a hybrid single-photon detector. Analysis of the measured exponential decay gives a lifetime of the $^1P_1$ state of $\tau = (5.216 \pm 0.006_{\text{stat}} \pm 0.013_{\text{sys}})$ ns, where all the systematic effects have been thoroughly considered.

DOI: 10.1103/PhysRevA.111.032809

I. INTRODUCTION

In the past two decades, strontium optical lattice clocks have continuously advanced the frontier in lowering accuracy uncertainty, with recent realizations reaching the 10^{-19} range [1]. These levels of accuracy not only put Sr as one of the leading candidate elements for the redefinition of the second [2], but also promise to advance geodesy [3–9] and impose constraints on dark matter models [10–14] and on the variation of fundamental constants [15,16].

The largest contribution to the uncertainty of state-of-the art Sr lattice clocks comes from the blackbody radiation (BBR) shift. This shift arises from considerable differential polarizability of the clock states $5s^2\,^1S_0$ and $5s5p\,^3P_0$ at wavelengths corresponding to the thermal radiation at room temperature at which these clocks typically operate. The static part of the polarizability, which scales as T^4, has been measured to such a high precision [17] that it contributes negligibly to the overall uncertainty. However, the dynamic part, which scales with higher powers of T, needs to be calculated from the available spectroscopic data and is the primary contributor to the BBR shift uncertainty [1,18–21]. This dynamic polarizability depends on the Einstein coefficients A between higher-lying states and the clock states. For the $5s^2\,^1S_0$ state, the dominant contribution, over 90% of the total polarizability, comes from the $5s5p\,^1P_1$ state. Therefore, a precise and accurate determination of $A(5s5p\,^1P_1 \rightarrow 5s^2\,^1S_0)$ is crucial for lowering the uncertainty of Sr lattice clocks.

The commonly used value was measured through photoassociation spectroscopy [22]. Here the authors mapped out the molecular state near the $5s^2\,^1S_0 + 5s5p\,^1P_1$ atomic asymptote by measuring the photoassociation spectrum. By fitting a dipole-dipole interaction model to the data, they extract the coupling constant C_3, which is directly proportional to the decay rate of the $5s5p\,^1P_1$ state. Alternatively, it can be calculated from the combination of measurements of the tune-out wavelength [23] and the lifetime of the $^3P_1$ state [1,19]. At this tune-out wavelength the dynamic polarizability of the $5s^2\,^1S_0$ ground state is zero due to it being red detuned from the $5s^2\,^1S_0 \rightarrow 5s5p\,^1P_1$ transition and blue detuned from the $5s^2\,^1S_0 \rightarrow 5s5p\,^3P_1$ transition. Since both exited states decay only to the ground state, the position of the tune-out wavelength is determined by the ratio of the corresponding decay rates τ^{-1}. This allows $\tau_{^1P_1}$ to be determined from the previously mentioned measurements. However, these two approaches show a 7σ disparity, an inconsistency also noted in [21].

In this paper we report on the measurement of the lifetime of the $5s5p\,^1P_1$ state in atomic Sr using femtosecond laser excitation and time-correlated single-photon counting (TCSPC). As a direct measurement of the lifetime, our result has the potential to resolve the previously mentioned 7σ disparity and contribute to a more precise calculation of the dynamic polarizability correction. This in turn will enable a more accurate calculation of the BBR shift, ultimately improving the precision of Sr lattice atomic clocks.

In our experiment, we generate an atomic beam in an under-vacuum spectroscopy cell using a dispenser, excite it with a femtosecond laser resonant with the $5s^2\,^1S_0 \rightarrow 5s5p\,^1P_1$ transition at approximately 461 nm, and collect the fluorescence onto a hybrid single-photon detector. By using the TCSPC method, we are able to measure individual photons emitted by atoms following the excitation with a femtosecond laser and record their arrival times with picosecond resolution [24]. Over many cycles of excitation and spontaneous emission, an exponential histogram of photon counts in time is recorded, with the time constant being the lifetime of the excited state.

Using a femtosecond laser emitting at approximately 461 nm, we achieve the necessary fast switch-off times shorter than the $5s5p\,^1P_1$ lifetime of approximately 5 ns. This approach allows us to bypass the need for electro-optic modulators, which are commonly used for fast switch-off of laser excitation at red and near-infrared wavelengths [25], but are unavailable for blue wavelengths, thus making the

*Present address: Instituto de Física de São Carlos, Universidade de São Paulo, São Carlos, SP 13566-970, Brazil.
†Contact author: nsantic@ifs.hr

 ©2025 American Physical Society

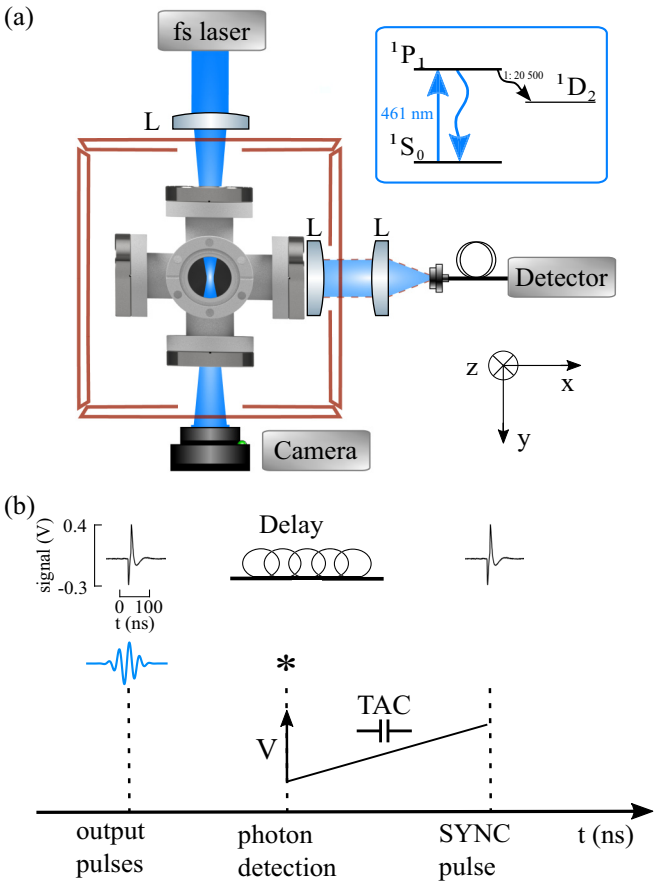

FIG. 1. (a) Simplified scheme of the experimental setup and relevant energy levels of strontium. The atomic beam of strontium atoms is propagating in the $-z$ direction and is produced using a dispenser in the center of the vacuum cell. (b) The optical pulse (sketched in blue) and the sync pulse (shown as recorded) originate simultaneously from the femtosecond laser. The optical pulse travels from the laser to the atoms, exciting them. The excited atoms then spontaneously emit photons, which are detected by the single-photon detector. This detection triggers the TAC, represented as a charging capacitor. To delay the sync pulse, we introduce 66 m of coaxial cable into its path, ensuring it arrives approximately 70 ns after the first detected photons. The sync pulse then stops the TAC, whose voltage is subsequently read by an ADC. See the text for more details.

measurements of short lifetimes in the blue spectrum technically challenging.

Our paper is organized as follows. Details of the experiment are given in Sec. II and our approach to the data analysis is in Sec. III. In Sec. IV we present our data and in Sec. V we discuss all the systematic effects contributing to the error budget of our measurement. We summarize in Sec. VI.

II. EXPERIMENTAL METHODS

A simplified scheme of the experimental setup and energy levels of strontium relevant to the measurement of the $^1P_1$ lifetime is shown in Fig. 1. Even though there is a probability of atom relaxation from the $^1P_1$ state to the $^1D_2$ state, this occurs only once per 20 500 photons [26] and is therefore negligible.

An atomic beam of hot strontium atoms is generated using a dispenser (AlfaVakuo, AS-Sr-5V-600) placed inside an under-vacuum (approximately 10^{-5} mbar) spectroscopy cell, similar in design to our previous work [27]. The dispensers are aligned along the z axis, with the atomic beam emerging from the dispenser approximately 3 mm below the x-y plane.

A diode-pumped Yb-doped potassium gadolinium tungstate. femtosecond laser (Light Conversion, Carbide) is used to excite the atoms. It propagates along the y axis, perpendicular to the atomic beam, and is focused at the center of the cell.

To estimate the atomic velocity distribution at the point where the femtosecond laser intersects the atomic beam, we direct a continuous-wave (cw) laser at 461 nm (Moglabs, CEL) along the same path as the femtosecond laser. We measure its transmission as a function of frequency by scanning over the $^1S_0$-$^1P_1$ transition, i.e., we measure the absorption spectrum. The resulting atomic velocity distribution closely resembles a Maxwell-Boltzmann distribution, with an estimated full width at half maximum (FWHM) of approximately approximately 1 GHz at a dispenser current of 9.5 A. Moreover, from transmission measurements using a cw laser and applying the Beer-Lambert law, we calculate the optical thickness of strontium atoms emerging from the dispensers at different currents.

The femtosecond laser operates at a nominal wavelength of 1030 nm, with a pulse duration of approximately 280 fs and a repetition rate of 1 MHz. To achieve the required excitation wavelength of 461 nm, the femtosecond pulses are directed through a hybrid optical parametric amplifier (OPA) (ORPHEUS-F-NS), followed by a pulse compressor and a second-harmonic generator (SHG). At the SHG output, a femtosecond laser spectrum centered at 461 nm with a FWHM of 17 nm is measured. Due to this broad laser bandwidth, most of the photons are off-resonance with the $^1S_0$-$^1P_1$ atomic transition at 461 nm. The spectrum is further filtered to a FWHM of 1.6 nm using an optical grating (Thorlabs, GH13-24V) combined with a vertical slit (Thorlabs, VA100CP/M).

The femtosecond beam has elliptical profile at the focus with $1/e^2$ diameters of 0.31 and 0.25 mm along the x and z axes, respectively, as measured using a beam profiler (Ophir Optronics Solutions, BM-USB-SP928-OSI). For the average power of 36 μW used in all measurements (unless otherwise noted) and assuming the pulse has a Gaussian envelope, along with the mean beam diameter and a pulse duration of 280 fs, we find a pulse area of 0.08π [28]. During lifetime measurements, the power of the femtosecond laser beam and its focal position are continuously monitored using a beam profiler. The data show that, across all lifetime measurements, the femtosecond laser power fluctuates within 4% of the total power, while the focal point position drifts up to 4 μm along the x axis and 22 μm along the z axis. While the measured changes are small, they do contribute to the background variations relevant for the lifetime measurements conducted over several days, as will be discussed in detail in Sec. III.

The photons emitted through spontaneous decay are coupled into a 400-μm-diam multimode optical fiber (Thorlabs, M74L05) using a telescope with a 5:1 focal ratio, resulting in a 2-mm-diam imaging area. The size of the imaging area

is made as large as possible so as to minimize transit-time broadening. Even atoms with velocities of 1000 m/s, a factor of approximately 2 more than the most likely velocity in the atomic beam, take 2 μs to cross the imaging area, which is two orders of magnitude longer than the time span of our decay curve. This means that the effect of transit-time broadening on our measurements is negligible. The optical fiber is 5 m long and guides the photons to a hybrid single-photon detector (Becker & Hickl, HPM-100-07). The detector is characterized by extremely low afterpulsing probability and quantum efficiency of approximately 15% at 461 nm. During lifetime measurements, the temperature of the detector is monitored using a temperature data logger (Pico Tech., TC-08). For all lifetime measurements performed, the detector temperature variations are less than 0.7 °C, ensuring that the dark counts remain constant throughout the measurements. For efficient single-photon arrival timing, a SPC-130-EMN TCSPC module with a timing precision of less than 3.5 ps and a dead time of 100 ns is used. To suppress stray light, such as room light or femtosecond laser light of other wavelengths used in the OPA and SHG, a bandpass filter centered at 460 nm (Thorlabs, FBH460-10) with a 10-nm FWHM is used in front of the detector.

In our measurements we use the reverse start-stop mode of TCSPC. In this mode, the time-to-amplitude converter (TAC) starts when a photon is detected and stops upon receiving a sync pulse from the laser. To ensure that the pulse exciting the atoms and producing the photon that starts the TAC is the same pulse that provides the sync to stop the TAC, we adjust the length of the sync cable. The length added is 66 m, resulting in an approximately 300 ns delay ensuring the sync pulse arrives approximately 70 ns after the first detected photons. This allows us to measure the arrival time of the detected photon relative to the laser pulse that caused the excitation, which eliminates the effects of the femtosecond pulse-period jitter.

All measurements are conducted within a time window of 66.025 ns, determined by adjusting the lengths of the constant fraction discriminator cable and the sync signal cable, and the TAC settings. This configuration, with the addition of the dead time of the detector of 100 ns, leaves more than 800 ns of detector readiness for the arrival of the next photon. As a result, the influence of the detector's dead time is entirely eliminated. The analog-to-digital converter (ADC) is set to its highest available resolution of 4096 bins, which provides a time-bin duration of 16.12 ps per bin.

Three pairs of bias coils are placed in three orthogonal directions (x, y, and z) around the cell to compensate for any stray magnetic field. The coils are significantly larger than the laser's interaction region with the strontium atoms, ensuring a homogeneous magnetic field within that area. The magnetic field is measured at multiple locations around the cell using a magnetometer (Sensys GmbH, FGM3D/1000). The field in the center of the cell, where the femtosecond laser interacts with the atoms, is estimated through interpolation. The magnetic field is reduced to zero with an error margin of 0.01 G, constrained by the sensitivity of the magnetometer. In all measurements, the magnetic field is set to zero unless the bias coils are intentionally used to generate a nonzero dc magnetic field. This nonzero field is applied to investigate the dependence of the atomic lifetime on the magnetic field, as detailed in Sec. V D.

For a given set of experimental parameters (Sr dispenser current, external magnetic field, femtosecond laser power, and focal position), measurements are conducted in the following order: First, the background is measured; then the signal, i.e., spontaneously emitted photons; and finally, the background is measured again.

We measure the background signal with the femtosecond laser tuned to approximately 457 nm, i.e., sufficiently detuned from the $^1S_0$-$^1P_1$ transition to avoid excitation of the atoms. Therefore, it includes both dark counts, and photons scattered and reflected from the interior and viewports of the spectroscopy cell, including dispensers. Due to multiple reflections, these photons can reach the detector well after the femtosecond excitation pulse has ended; in our case, their presence is detectable in the background signal for up to approximately 7.5 ns. After this time the signal decreases by five orders of magnitude and is dominated by the photon dark count. This extinction ratio is far better than what is typically achievable by using an electro-optical modulator [25]. Furthermore, we observe no decay signal that could possibly be due to off-resonance excitation. In each measurement sequence, we ensure that the total background signal measurement time (taken before and after signal) matches the duration of the on-resonance signal measurement. Measuring the background signal before and after the on-resonance signal enables us to estimate the error in the lifetime measurement caused by background fluctuations, which can arise from slight variations in the femtosecond laser intensity and focal position.

III. DATA ANALYSIS

A. Pulse pileup correction

Each measured data set (both background and signal) is first corrected for pulse pileup, which occurs when more than one spontaneously emitted photon reaches the detector within a single excitation cycle. In such cases, the TCSPC registers the first photon but fails to register subsequent ones, which results in undercounting in later time bins. The pileup correction is made by multiplying the number of detected photon counts N_i in time bin i by a factor defined as [29]

$$F_i = \frac{1}{1 - \frac{1}{N_E}\sum_{j<i-1} N_j}, \tag{1}$$

where N_E is the number of excitation cycles and N_j is the number of photon counts collected in the jth time bin. The largest correction factor, of approximately 1.028, is obtained for the signal measured at the highest strontium optical depth, where the photon counts is approximately 2.7% of the repetition rate.

B. Fitting

For a given signal data set, after correcting the collected photon counts for the pileup effect, we fit an exponential function of the form

$$N(t) = A\exp(-t/\tau) + p[B_1(t) + B_2(t)], \tag{2}$$

where τ is the exponential decay time constant corresponding to the lifetime of the $^1P_1$ state, A is the amplitude of the

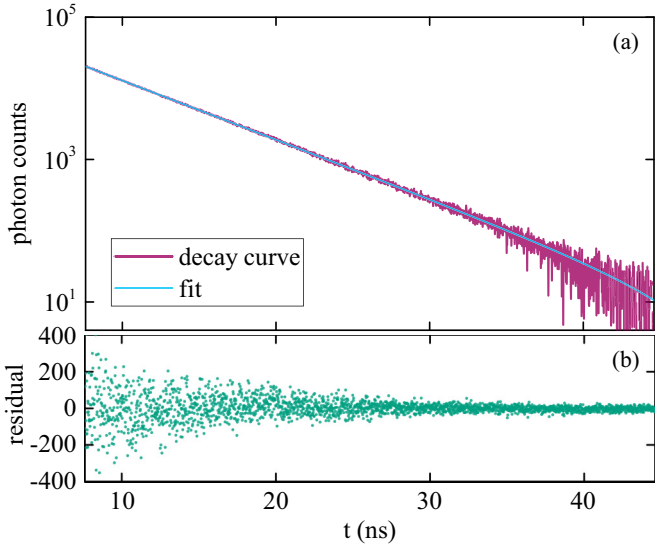

FIG. 2. (a) Fluorescence decay curve of the $^1P_1$ state (pink) with the background signal removed. The corresponding decay curve that is the result of our fitting procedure is shown in blue. Note that the fitting function also includes the background signal, which is not shown here. See the text for more details about the fitting procedure. (b) Fit residuals.

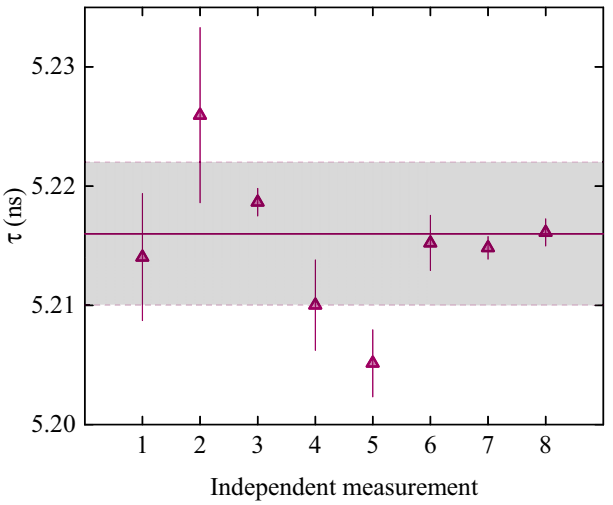

FIG. 3. Lifetime of the $^1P_1$ state determined from eight independent measurements. For data sets 1, 4, and 8, the signal was collected over 23, 38, and 20 h, respectively, while the remaining data sets were collected over 15 h. The error bars are calculated by adding the fit error, the truncation, and the background error in quadrature for each data set. The horizontal line represents the weighted mean of the eight data sets, with the gray shaded area indicating the standard deviation.

exponential function, and $B_1(t)$ and $B_2(t)$ are background signals measured before and after the decay signal, respectively. The total background signal $B_1(t) + B_2(t)$ accounts for the dark counts and for photons reflected from the interior of the spectroscopy cell, including dispensers. However, as noted earlier, the contribution of photons reflected from the cell interior to the background signal decreases by five orders of magnitude from its peak within just 7.5 ns, after which the background is primarily dominated by dark counts. Additionally, it is important to emphasize that the background acquisition time, for backgrounds measured both before (B_1) and after (B_2) the signal measurement, is always equal to the signal acquisition time. Consequently, the fitting parameter p from Eq. (2), which scales the background signals to account for potential fluctuations during the acquisition time, typically deviates from 1 by only a few percent across all measurements.

An example of a decay signal is shown in Fig. 2(a), where the background signal, multiplied by the fitting parameter p, has been subtracted. The exponential decay part of the fitted function $A\exp(-t/\tau)$ is shown in blue. The residuals are shown in Fig. 2(b) and are consistent with the shot noise corresponding to the signal level.

Although the fitting curve, according to the relation (2), also includes the background, we observe that the obtained lifetime τ significantly depends on the starting bin time of the fit. Determining the adequate start bin time of the fit, commonly referred to as the truncation time, is not straightforward and requires a systematic approach [30,31]. In our approach, we use the measured signal data set to generate multiple data sets for the fit, each with a different truncation time. The difference in truncation times between two consecutive data sets is 0.5 ns. We then perform a global fit, simultaneously fitting all data sets, each with a different truncation time, to a single function given by Eq. (2), where the parameters A and p are shared across all data sets. Thus we obtain a set of τ_i values from the fit, each corresponding to the same measured signal data set, but using different truncation time for the fit. We limit the fit to the range from the selected truncation time up to $t = 44.6$ ns, the point at which the photon count in the signal corresponds to the dark count level. The global fit code is run using *Mathematica* [32]. We analyze the obtained τ_i values for different truncation times and find that when the truncation time is set between 7.6 and 10.6 ns, τ_i remains constant, indicating no dependence on the choice of the fit's start time. The final τ for a given measured signal data set is determined as the mean of τ_i values obtained from the global fit within this truncation interval. To estimate the uncertainty in τ for a given measured data set, we calculate the standard deviation of τ_i values across the selected truncation interval, which we refer to as the truncation uncertainty. We then add in quadrature the largest fit error within this interval and the background error to determine the total uncertainty in τ for the measured data set. The background error is estimated using again Eq. (2) as the fit function; however, now only B_1 or B_2 are used, rather than their sum $B_1 + B_2$. We define the background error as half the difference of τ_{B_1} and τ_{B_2} obtained in this way. The background error reflects variations in τ caused by small changes in the background during signal measurement.

IV. LIFETIME OF THE $5s5p\,^1P_1$ STATE

In Fig. 3 we present the $^1P_1$ state lifetime obtained from eight independent measurements conducted under identical experimental conditions on different days over a two-month period. For measurements denoted by numbers 1, 4, and 8, the

TABLE I. Error budget of the $^1P_1$ state lifetime measurement.

Error source	Uncertainty (%)
TAC nonlinearity	0.2
Magnetic field	0.004
Radiation trapping	0.096
Total systematic error	0.25
Statistical error	0.115

signal is collected over 23, 38, and 20 h, respectively, while the remaining data sets are collected over 15 h. The optical depth of the atomic sample is 0.0011, estimated as described in Sec. II. The lifetime of the $^1P_1$ state and corresponding uncertainties are determined for each data set as explained in Sec. III. The background error is the largest contributor to τ uncertainty for a particular data set. The average truncation error is 0.008%, while the maximum fitting error is 0.017%. From these eight independent measurements and their uncertainties, the lifetime of the $5s5p\,^1P_1$ state is determined by calculating the weighted mean, resulting in $\tau = 5.216$ ns, with a standard deviation, here referred to as the statistical error, of 0.006 ns (see Fig. 3).

V. SYSTEMATIC EFFECTS

Accurate determination of the lifetime of the $^1P_1$ state requires a rigorous investigation of the systematic effects that could influence our result. We thoroughly examined all potential sources of uncertainty in τ, including signal nonuniformity, nonlinearity of the TAC, femtosecond laser power, magnetic field, and radiation trapping. We summarize the contribution of these effects in the error budget in Table I.

After carefully considering each of these contributions and including them in our result, we estimate the total uncertainty in the lifetime measurement to be 0.25%, which yields the final lifetime of the $^1P_1$ state of

$$\tau(^1P_1) = (5.216 \pm 0.006_{\text{stat}} \pm 0.013_{\text{sys}})\ \text{ns}. \tag{3}$$

A detailed description of each contribution is provided below.

A. Signal nonuniformity

To test the signal nonuniformity of the ADC bins we collect scattered light from a cw laser at 461 nm. The laser power is adjusted so that the photon count rate matches the rate used in the lifetime measurements. Over an acquisition time of approximately 20 min, around 5000 photons per bin are collected. Since we are now using a cw source, i.e., a non-time-correlated source, we expect a uniform signal in all time bins. However, we find a small increase in counts with time. With a maximal time window of 1 μs, we find that the bins at the end of the window have on average 20 counts, or 0.4%, more than the ones at the beginning, with an overall linear slope across the time window. We attribute this nonuniformity to time-correlated electronic noise in the signal acquisition system. For the time window used for the decay rate data, 66.025 ns, this corresponds to 1.3 counts, two orders of magnitude lower than the typical dark noise level in our data. Therefore, we conclude that the signal nonuniformity does not contribute to the total error of our measurement.

B. TAC nonlinearity

To determine time calibration errors in the TAC, two pulses, i.e., a start and a stop, are sent to the SPC-130-EMN TCSPC module using a digital delay generator (SRS, DG645). Additionally, the generated pulses are calibrated by a time interval counter (Keysight, 53220A). Varying the delay between the pulses while observing the TAC's output and applying a linear fit to the data, we observe a slope different from the expected one-to-one correspondence. The measured slope varies slightly from day to day, with the maximal observed slope being 1.002 40(4). This indicates a small but measurable deviation from ideal linear behavior of the TAC. Effectively, this means that the slope of the decay curve would be smaller than measured, implying that the actual lifetime is shorter. To estimate the contribution to the uncertainty, we multiply time bins of a data set with the highest measured slope and fit using the mentioned fitting procedure. We take the difference between this lifetime and the one obtained with no multiplication as the contribution to the uncertainty, equaling 0.2% of the measured lifetime value.

C. Laser power

Minor fluctuations in laser power during fluorescence decay measurements cause slight changes in the background during signal acquisition, affecting the accuracy of the fit used to determine τ. This effect, referred to as the background error, is estimated for each individual data set, as detailed in Sec. III, and is included in the statistical error.

Another potential effect of laser power on lifetime could stem from spectral line broadening and saturation. Although our measurements are performed at low laser powers, resulting in low photon count rates, we evaluate this contribution as well. We measure the signals and corresponding backgrounds for four different femtosecond laser power, keeping all other experimental parameters constant. The femtosecond laser powers are 7, 36, 66, and 68 μW. Using the measured data and following the procedure described above, we determine τ for each data set measured at different femtosecond laser powers. The uncertainty for each τ value is calculated by combining truncation, fit, and background errors in quadrature. All obtained τ values fall within the calculated statistical uncertainty range $\tau = 5.216 \pm 0.006$ ns, indicating no dependence of τ on laser power within the power range used.

D. Magnetic field

In the presence of an external static magnetic field, the $^1P_1$ state splits into three Zeeman components $m_J = 0, \pm 1$. The splitting between these components is given by $E_{ZE} = g_J \mu_B M_J B$, where g_J is the Landé g factor, μ_B is the Bohr magneton, m_J is the magnetic quantum number, and B is the magnetic-field strength that has a value of 1.4 MHz/G.

Given the spectral width of the femtosecond laser, coherent excitation of the three Zeeman components of the $^1P_1$ excited state is possible, potentially leading to interference among the different $^1P_1$ $(m_J = \pm 1, 0)$–$^1S_0$ $(m_J = 0)$ decay paths. This

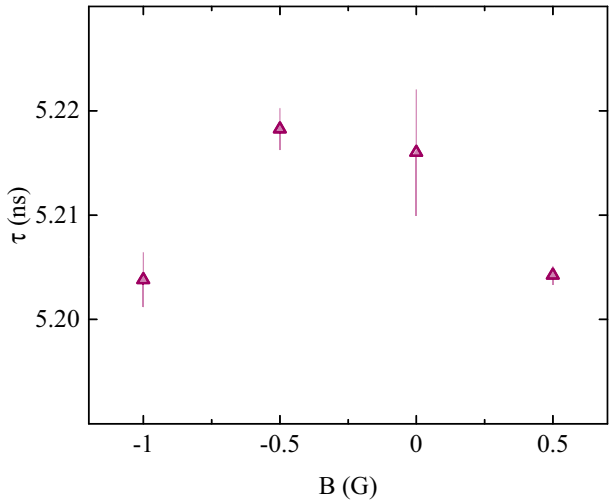

FIG. 4. Measured lifetime of the $^1P_1$ state for various external magnetic-field strengths.

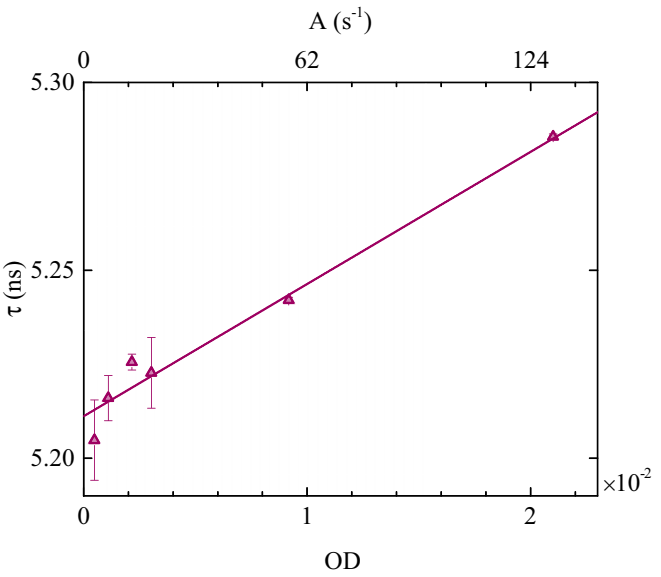

FIG. 5. Measured lifetime of the $^1P_1$ state across a range of strontium optical depths (symbols). The solid line is a linear fit to data and yields an extrapolated lifetime of 5.211 ns for zero Sr density, with a fitting uncertainty of 0.002 ns. The corresponding parameter A is given on the upper x axis.

effect is known as quantum beats and causes the exponential decay function to be modulated by a cosine function [30,33], making Eq. (2) no longer a suitable fit for the measured data. The frequency of the modulation cosine function is equal to E_{ZE}/h, where h is Planck's constant.

In our experimental setup, the magnetic field at the center of the cell, within the interaction zone of atoms and the femtosecond laser, is zeroed to an accuracy of 0.01 G (see Sec. II). At this field strength, the period of the cosine function that modulates the exponential function due to quantum beats is 36 μs, which is four orders of magnitude longer than the measured time window relevant for the determination of the $^1P_1$ state lifetime. Thus, we estimate that for measurements performed at 0 G, the effect of the modulation of the exponential fitting function by cosine function is negligible, resulting in no added uncertainty in τ related to the quantum beat effects.

To confirm this conclusion, we introduce an external static magnetic field to the interaction zone of the femtosecond laser and strontium atoms and measure the dependence of τ on the applied magnetic field, keeping all other experimental parameters constant. The external magnetic field is introduced along the y axis, i.e., parallel to the laser propagation vector, using a pair of coils described in Sec. II. Using the measured data and the global fitting procedure described above, we determine τ for each data set measured at different magnetic-field strength. The uncertainty for each τ value is calculated by combining truncation, background, and fit errors in quadrature. Figure 4 presents the results, showing a certain dependence of τ on the strength of the external magnetic field; however, this dependence does not follow a straightforward functional form.

To conservatively estimate the uncertainty in τ near $B = 0$, we use the largest observed deviation in τ across the measured magnetic-field range. The largest deviation, measured at $B = 0.5$ G, is 0.19% relative to τ at $B = 0$. From this, we estimate that the deviation at $B = 0.01$ G, corresponding to the accuracy of the magnetic field measured at $B = 0$, is approximately 0.004%. Although this is negligible compared to other sources of τ uncertainty, we have included it in the error budget table.

E. Radiation trapping

In dense vapors, the observed lifetime increases due to radiation trapping [34–36]. To evaluate the influence of this effect, we measure the lifetime of the $^1P_1$ state at various optical depths (ODs) of strontium vapor in the cell. We adjust the OD by changing the current through the dispenser. Optical depth measurements are performed using the aforementioned cw laser at 461 nm. For a given dispenser current, we record the transmission of the cw laser as a function of its frequency by scanning across the $^1S_0$-$^1P_1$ transition, effectively measuring the absorption spectrum. From these data we calculate the OD for each current setting using the Lambert-Beer law. For dispenser currents below 8.5 A, direct OD measurements are challenging due to low absorption resulting from the low strontium atom concentration. In these cases, we estimate the OD from the fit parameter A, which is confirmed to correlate with the concentration of strontium atoms. To quantify this, we plot A as a function of OD for the measurable OD range, obtaining a linear relationship. These fit parameters are then used to calculate OD from the photon count rate for cases with lower dispenser currents.

Figure 5 shows measurements of τ as a function of OD. For completeness, the corresponding parameter A is given on the upper x axis. A linear dependence of τ vs OD is found, consistent with previous literature [34–36]. The linear fit to data yields an extrapolated lifetime of 5.211 ns for zero Sr density, with a fitting uncertainty of 0.002 ns. This results in a correction of 0.096% for the lifetime of 5.216 ns, measured at an OD of 0.0011 from eight independent measurements.

VI. CONCLUSION

To conclude, we have measured the lifetime of the $^1P_1$ state in Sr using the TSCPC technique. Additionally, we carefully analyzed systematic effects that affect our measurements. The largest contribution to the uncertainty, the TAC nonlinearity, could be drastically reduced by using another type of time-to-digital converter, for instance, a field-programmable gate array [37]. Nevertheless, our final result $\tau(^1P_1) = (5.216 \pm 0.006_{\text{stat}} \pm 0.012_{\text{sys}})$ ns has a comparable error to previous measurements [22,23]. As mentioned, these two previous measurements show a 7σ discrepancy. Our result agrees within σ with the result obtained by Heinz *et al.* [23] from a tune-out frequency measurement, providing new and valuable information regarding the issue of the discrepancy with the lifetime determined from photoassociation spectroscopy [22]. The reported error in [22] represents only the fitting uncertainty. Therefore, uncharacterized systematic effects may have influenced the obtained lifetime. For example, the authors used a high-intensity photoassociation laser at 10 W/cm^2, or approximately $240I_{\text{sat}}$, and the line shape is expected be influenced by such high intensities [38]. Other possible systematic effects were discussed in [39], which describes a similar photoassociation measurement. We expect that this new spectroscopic data will improve the accuracy of calculations of the internal structure of the strontium atom, ultimately leading to more accurate strontium atomic clocks. However, the full evaluation of the potential accuracy improvement depends on the consistency of our result and other available spectroscopic data used in models of the strontium atom used to determine the BBR shift, such as in [21].

ACKNOWLEDGMENTS

We thank G. Zgrablić and S. Vdović for their support in operating the femtosecond laser. This work was supported by the following projects: New Imaging and Control Solutions for Quantum Processors and Metrology, funded within the QuantERA II Programme that has received funding from the DEU H2020 research and innovation programme under GA No 101017733, and with funding organisations Croatian Science Foundation HrZZ, Federal Ministry of Education and Research BMBF, Association of German Engineers Technology center VDI TZ and National Center for Research and Development NCBR; Croatian Quantum Communication Infrastructure, funded through Digital Europe Call (Projects No. 101091513 and No. NPOO.C3.2.R2-12.01.0001); and Centre for Advanced Laser Techniques, cofunded by the European Union through the European Regional Development Fund under the Competitiveness and Cohesion Operational Programme (Grant No. KK.01.1.1.05.0001).

DATA AVAILABILITY

The data that support the findings of this article are available within the publication [40].

[1] A. Aeppli, K. Kim, W. Warfield, M. S. Safronova, and J. Ye, Clock with 8×10^{-19} systematic uncertainty, Phys. Rev. Lett. **133**, 023401 (2024).

[2] N. Dimarcq, M. Gertsvolf, G. Mileti, S. Bize, C. W. Oates, E. Peik, D. Calonico, T. Ido, P. Tavella, F. Meynadier, G. Petit, G. Panfilo, J. Bartholomew, P. Defraigne, E. A. Donley, P. O. Hedekvist, I. Sesia, M. Wouters, P. Dubé, F. Fang *et al.*, Roadmap towards the redefinition of the second, Metrologia **61**, 012001 (2024).

[3] T. E. Mehlstäubler, G. Grosche, C. Lisdat, P. O. Schmidt, and H. Denker, Atomic clocks for geodesy, Rep. Prog. Phys. **81**, 064401 (2018).

[4] J. Grotti, S. Koller, S. Vogt, S. Häfner, U. Sterr, C. Lisdat, H. Denker, C. Voigt, L. Timmen, A. Rolland, F. N. Baynes, H. S. Margolis, M. Zampaolo, P. Thoumany, M. Pizzocaro, B. Rauf, F. Bregolin, A. Tampellini, P. Barbieri, M. Zucco *et al.*, Geodesy and metrology with a transportable optical clock, Nat. Phys. **14**, 437 (2018).

[5] J. Grotti, I. Nosske, S. Koller, S. Herbers, H. Denker, L. Timmen, G. Vishnyakova, G. Grosche, T. Waterholter, A. Kuhl, S. Koke, E. Benkler, M. Giunta, L. Maisenbacher, A. Matveev, S. Dörscher, R. Schwarz, A. Al-Masoudi, T. Hänsch, T. Udem *et al.*, Long-distance chronometric leveling with a portable optical clock, Phys. Rev. Appl. **21**, L061001 (2024).

[6] M. Takamoto, I. Ushijima, N. Ohmae, T. Yahagi, K. Kokado, H. Shinkai, and H. Katori, Test of general relativity by a pair of transportable optical lattice clocks, Nat. Photon. **14**, 411 (2020).

[7] Y. Huang, H. Zhang, B. Zhang, Y. Hao, H. Guan, M. Zeng, Q. Chen, Y. Lin, Y. Wang, S. Cao, K. Liang, F. Fang, Z. Fang, T. Li, and K. Gao, Geopotential measurement with a robust, transportable Ca^+ optical clock, Phys. Rev. A **102**, 050802(R) (2020).

[8] T. Bothwell, C. J. Kennedy, A. Aeppli, D. Kedar, J. M. Robinson, E. Oelker, A. Staron, and J. Ye, Resolving the gravitational redshift across a millimetre-scale atomic sample, Nature (London) **602**, 420 (2022).

[9] X. Zheng, J. Dolde, M. C. Cambria, H. M. Lim, and S. Kolkowitz, A lab-based test of the gravitational redshift with a miniature clock network, Nat. Commun. **14**, 4886 (2023).

[10] A. Derevianko and M. Pospelov, Hunting for topological dark matter with atomic clocks, Nat. Phys. **10**, 933 (2014).

[11] A. Arvanitaki, J. Huang, and K. Van Tilburg, Searching for dilaton dark matter with atomic clocks, Phys. Rev. D **91**, 015015 (2015).

[12] K. Beloy, M. I. Bodine, T. Bothwell, S. M. Brewer, S. L. Bromley, J.-S. Chen, J.-D. Deschênes, S. A. Diddams, R. J. Fasano, T. M. Fortier, Y. S. Hassan, D. B. Hume, D. Kedar, C. J. Kennedy, I. Khader, A. Koepke, D. R. Leibrandt, H. Leopardi, A. D. Ludlow, W. F. McGrew *et al.*, Frequency ratio measurements at 18-digit accuracy using an optical clock network, Nature (London) **591**, 564 (2021).

[13] N. Sherrill, A. O. Parsons, C. F. A. Baynham, W. Bowden, E. A. Curtis, R. Hendricks, I. R. Hill, R. Hobson, H. S. Margolis, B. I. Robertson, M. Schioppo, K. Szymaniec, A. Tofful, J. Tunesi, R. M. Godun, and X. Calmet, Analysis of atomic-clock data to constrain variations of fundamental constants, New J. Phys. **25**, 093012 (2023).

[14] M. Filzinger, S. Dörscher, R. Lange, J. Klose, M. Steinel, E. Benkler, E. Peik, C. Lisdat, and N. Huntemann, Improved limits on the coupling of ultralight bosonic dark matter to photons from optical atomic clock comparisons, Phys. Rev. Lett. **130**, 253001 (2023).

[15] M. S. Safronova, D. Budker, D. DeMille, D. F. J. Kimball, A. Derevianko, and C. W. Clark, Search for new physics with atoms and molecules, Rev. Mod. Phys. **90**, 025008 (2018).

[16] G. Barontini, L. Blackburn, V. Boyer, F. Butuc-Mayer, X. Calmet, J. R. C. López-Urrutia, E. A. Curtis, B. Darquié, J. Dunningham, N. J. Fitch, E. M. Forgan, K. Georgiou, P. Gill, R. M. Godun, J. Goldwin, V. Guarrera, A. C. Harwood, I. R. Hill, R. J. Hendricks, M. Jeong *et al.*, Measuring the stability of fundamental constants with a network of clocks, EPJ Quantum Technol. **9**, 12 (2022).

[17] T. Middelmann, S. Falke, C. Lisdat, and U. Sterr, High accuracy correction of blackbody radiation shift in an optical lattice clock, Phys. Rev. Lett. **109**, 263004 (2012).

[18] M. S. Safronova, S. G. Porsev, U. I. Safronova, M. G. Kozlov, and C. W. Clark, Blackbody-radiation shift in the Sr optical atomic clock, Phys. Rev. A **87**, 012509 (2013).

[19] T. L. Nicholson, S. L. Campbell, R. B. Hutson, G. E. Marti, B. J. Bloom, R. L. McNally, W. Zhang, M. D. Barrett, M. S. Safronova, G. F. Strouse, W. L. Tew, and J. Ye, Systematic evaluation of an atomic clock at 2×10^{-18} total uncertainty, Nat. Commun. **6**, 6896 (2015).

[20] R. Hobson, W. Bowden, A. Vianello, A. Silva, C. F. A. Baynham, H. S. Margolis, P. E. G. Baird, P. Gill, and I. R. Hill, A strontium optical lattice clock with 1×10^{-17} uncertainty and measurement of its absolute frequency, Metrologia **57**, 065026 (2020).

[21] C. Lisdat, S. Dörscher, I. Nosske, and U. Sterr, Blackbody radiation shift in strontium lattice clocks revisited, Phys. Rev. Res. **3**, L042036 (2021).

[22] M. Yasuda, T. Kishimoto, M. Takamoto, and H. Katori, Photoassociation spectroscopy of ^{88}Sr: Reconstruction of the wave function near the last node, Phys. Rev. A **73**, 011403(R) (2006).

[23] A. Heinz, A. J. Park, N. Šantić, J. Trautmann, S. G. Porsev, M. S. Safronova, I. Bloch, and S. Blatt, State-dependent optical lattices for the strontium optical qubit, Phys. Rev. Lett. **124**, 203201 (2020).

[24] W. Becker, *The bh TCSPC Handbook*, 10th ed. (Becker & Hickl, Berlin, 2023).

[25] M. O. Araújo, I. Krešić, R. Kaiser, and W. Guerin, Superradiance in a large and dilute cloud of cold atoms in the linear-optics regime, Phys. Rev. Lett. **117**, 073002 (2016).

[26] A. Cooper, J. P. Covey, I. S. Madjarov, S. G. Porsev, M. S. Safronova, and M. Endres, Alkaline-earth atoms in optical tweezers, Phys. Rev. X **8**, 041055 (2018).

[27] A. Cipriš, I. Puljić, D. Aumiler, T. Ban, and N. Šantić, Absolute frequency measurement of the 5s5p $^1P_1$ - 5s5d $^1D_2$ transition in strontium, Spectrochim. Acta B **216**, 106942 (2024).

[28] D. Felinto, C. Bosco, L. Acioli, and S. Vianna, Coherent accumulation in two-level atoms excited by a train of ultrashort pulses, Opt. Commun. **215**, 69 (2003).

[29] E. Gomez, F. Baumer, A. D. Lange, G. D. Sprouse, and L. A. Orozco, Lifetime measurement of the 6*s* level of rubidium, Phys. Rev. A **72**, 012502 (2005).

[30] G. Toh, N. Chalus, A. Burgess, A. Damitz, P. Imany, D. E. Leaird, A. M. Weiner, C. E. Tanner, and D. S. Elliott, Measurement of the lifetimes of the $7p\,^2P_{3/2}$ and $7p\,^2P_{1/2}$ states of atomic cesium, Phys. Rev. A **100**, 052507 (2019).

[31] J. E. Simsarian, L. A. Orozco, G. D. Sprouse, and W. Z. Zhao, Lifetime measurements of the $7p$ levels of atomic francium, Phys. Rev. A **57**, 2448 (1998).

[32] S. Smit, MultiNonlinearModelFit, available at https://resources.wolframcloud.com/FunctionRepository/resources/MultiNonlinearModelFit.

[33] J. Brandenberger and B. Rose, Quantum beat determination of lifetimes and disalignment cross sections in neon, Opt. Commun. **36**, 453 (1981).

[34] E. A. Milne, The diffusion of imprisoned radiation through a gas, J. Lond. Math. Soc. **s1-1**, 40 (1926).

[35] B. M. Patterson, J. F. Sell, T. Ehrenreich, M. A. Gearba, G. M. Brooke, J. Scoville, and R. J. Knize, Lifetime measurement of the cesium $6P_{3/2}$ level using ultrafast pump-probe laser pulses, Phys. Rev. A **91**, 012506 (2015).

[36] S. Pucher, P. Schneeweiss, A. Rauschenbeutel, and A. Dareau, Lifetime measurement of the cesium $5\,^2D_{5/2}$ state, Phys. Rev. A **101**, 042510 (2020).

[37] J. Song, Q. An, and S. Liu, A high-resolution time-to-digital converter implemented in field-programmable-gate-arrays, IEEE Trans. Nucl. Sci. **53**, 236 (2006).

[38] E. Ribeiro, A. Zanelatto, and R. Napolitano, High-intensity and ground-state influence on photoassociation line shapes of ^{88}Sr, Chem. Phys. Lett. **390**, 89 (2004).

[39] S. B. Nagel, P. G. Mickelson, A. D. Saenz, Y. N. Martinez, Y. C. Chen, T. C. Killian, P. Pellegrini, and R. Côté, Photoassociative spectroscopy at long range in ultracold strontium, Phys. Rev. Lett. **94**, 083004 (2005).

[40] N. Šantić, Raw data for the lifetime measurement of the 5s5p 1P1 state in strontium (Harvard Dataverse, 2025).